Rom J Morphol Embryol 2020, 61(4):1235–1247 ISSN (print) 1220–0522, ISSN (online) 2066–8279 doi: 10.47162/RJME.61.4.25

ORIGINAL PAPER

RJME Romanian Journal of Morphology & Embryology http://www.rjme.ro/

Calcium fructoborate coating of titanium–hydroxyapatite implants by chemisorption deposition improves implant osseointegration in the femur of New Zealand White rabbit experimental model

RENATA-MARIA VĂRUŢ[1)], PETRU RĂZVAN MELINTE[2)], ANDREEA SILVIA PÎRVU[3)], OANA GÎNGU[4)], GABRIELA SIMA[4)], CARMEN NICOLETA OANCEA[5)], ALINA CRISTINA TEIŞANU[4)], GHEORGHE DRĂGOI[6)], ANDREI BIŢĂ[7,8)], HORIA OCTAVIAN MANOLEA[9)], IOANA MITRUŢ[3,9)], OTILIA CONSTANTINA ROGOVEANU[10)], ION ROMULUS SCOREI[8)], JOHNY NEAMŢU[11)]

[1)]*Department of Research Methodology, University of Medicine and Pharmacy of Craiova, Romania*

[2)]*Department of Orthopedics and Traumatology, University of Medicine and Pharmacy of Craiova, Romania*

[3)]*PhD Student, Doctoral School, University of Medicine and Pharmacy of Craiova, Romania*

[4)]*Department of Systems Engineering and Management Technology, Faculty of Mechanics, University of Craiova, Romania*

[5)]*Department of Analytical Chemistry, University of Medicine and Pharmacy of Craiova, Romania*

[6)]*Department of Anatomy, University of Medicine and Pharmacy of Craiova, Romania*

[7)]*Department of Pharmacognosy & Phytotherapy, Faculty of Pharmacy, University of Medicine and Pharmacy of Craiova, Romania*

[8)]*Department of Biochemistry, BioBoron Research Institute, S.C. Natural Research S.R.L., Podari, Dolj County, Romania*

[9)]*Department of Dental Materials, University of Medicine and Pharmacy of Craiova, Romania*

[10)]*Department of Physical Medicine and Rehabilitation, University of Medicine and Pharmacy of Craiova, Romania*

[11)]*Department of Physics, University of Medicine and Pharmacy of Craiova, Romania*

Abstract

Background: The identification of biocomposites that improve cell adhesion and reduce bone integration time is a great challenge for implantology and bone reconstruction. *Aim*: Our aim was to evaluate a new method of chemisorption deposition (CD) for improving the biointegration of hydroxyapatite-coated titanium (HApTi) implants. CD method was used to prepare a calcium fructoborate (CaFb) coating on a HApTi (HApTiCaFb) implant followed by evaluation of histological features related to bone healing at the interface of a bioceramic material in an animal model. *Methods*: The coating composition was investigated by high-performance thin-layer chromatography/mass spectrometry. The surface morphology of the coating was studied by scanning electron microscopy (SEM), before and after the *in vitro* study. We implanted two types of bioceramic cylinders, HApTi and HApTiCaFb, in the femur of 10 New Zealand White (NZW) rabbits. *Results*: The release of CaFb from HApTiCaFb occurred rapidly within the first three days after phosphate-buffered saline immersion; there was then a linear release for up to 14 days. SEM analysis showed similar morphology and particle size diameter for both implants. Around the porous HApTiCaFb implant, fibrosis and inflammation were not highlighted. *Conclusions*: Easily applied using CD method, CaFb coatings promote HApTi implant osseointegration in the femur of NZW rabbits.

Keywords: calcium fructoborate, hydroxyapatite, titanium implant, osseointegration, experimental model.

Introduction

There is growing interest in obtaining biomaterials for reconstructing bone tissue. Unwanted outcomes of post-implantation include assimilation of the implant, creation of proteolytic enzymes, and pro-inflammatory mediators and that form a granuloma around the implant, producing a series of biochemical reactions leading to osteolysis and bone resorption. Therefore, when considering metal implants or composites, there is the need for compatibility with the bone structure [1, 2].

Hydroxyapatite (HAp) is a biomaterial that exhibits biocompatibility and bioactivity; it is frequently used for bone grafting and coating orthopedic metallic components [3]. After implantation, it produces chemical species that promotes the adhesion of the implant to the surrounding tissue by forming a functional connective structure [4]. However, there are some major drawbacks of pure HAp, including its poor mechanical properties and the challenging preparation of harder HAp ceramic composites. Reinforcement with particles, whiskers, and long fibers have been used to make HAp composites with superior mechanical properties. Bio-inert metal particles of titanium (Ti) are useful for reinforcing HAp, having a positive

effect on mechanical and biological properties of the composites [5].

Calcium fructoborate (CaFb; $Ca[(C_6H_{10}O_6)_2B]_2 \bullet 4H_2O$) is a superoxide anion scavenger and anti-inflammatory agent, as shown by several *in vitro* studies [6]. Many research studies have reported that CaFb positively influences calcium metabolism, growth, and development of bone, soft tissues, and the formation of antibodies and collagen [7]. Given these considerations, combining Ti to reinforce HAp materials with active components, such as CaFb, may lead to new bone substitutes that successfully combine the properties of these classes of materials [8].

Aim

In the present study, we aimed to evaluate the osteo-formation after femoral implantation of rabbits with two types of bioceramic cylinders, hydroxyapatite-coated titanium (HApTi) and CaFb coating on a HApTi (HApTiCaFb) implant.

Materials and Methods

Design and fabrication of implanted cylinders

The biocomposite implant preparation was described thoroughly in our previous work [9–12]. In short, the matrix was produced from HAp powdered particles with an average size of 200 nm (Merck, Darmstadt, Germany) and reinforced with titanium hydride (TiH_2) particles of approximately 100 μm (Merck) in a 75:25 ratio (HAp, TiH_2). A couple of steps were conducted to obtain the final form implants. The first stage was to dry the HAp particles and strengthen them with the TiH_2, while the second phase was to compact and submit to a two-step sintering (TSS) heat process. After the sintered samples were obtained, one set was dipped into a CaFb stock solution, and another was left untreated as control [9–12].

Preparation of CaFb coating by chemisorption deposition

To examine potential ways to improve the osseo-integration of the biocomposite samples into genuine bone, some sintered samples were immersed into a CaFb-based solution. The CaFb is well recognized as a biomaterial with considerable benefits for the human body, not only from the nutritional perspective but also therapeutically. Recent research shows that CaFb may be used as a bio-adhesive to produce biocompatible implants, as well as an osseoinductive factor owing to its anti-inflammatory and antioxidative properties. The thermal behavior of CaFb was studied in previous research [13].

Solvents and reagents

Chromatographic grade solvents and reagents, such as Ethanol (99%), 2-Propanol, Water and Methanol (LiChrosolv®) were purchased from Merck (Darmstadt), and Chlorogenic Acid and Ammonium Acetate were obtained from Sigma-Aldrich (Munich, Germany). VDF FutureCeuticals (Momence, Illinois, USA) provided the CaFb standard (2.7%, expressed in boron).

Chemisorption deposition

The HApTi cylinders were immersed in CaFb solution (0.4 g/10 mL). The cylinders were weighed before and after chemisorption deposition (CD), after preliminary drying for 24 hours, at 20°C.

CaFb release and mass spectrometry confirmation

Cylinders were first immersed in sealed containers with 10 mL phosphate-buffered saline (PBS), at 37±0.5°C, for 15 days. At regular time intervals, 0.5 mL of solution was taken and immediately replaced with an equal volume of PBS. The amount of released CaFb was determined by the high-performance thin-layer chromatography (HPTLC) method [14]. To confirm that the compound truly was CaFb, we eluted one of the bands from the sample directly into the mass spectrometer and we obtained the expected mass spectrum [6]. The settings used for mass spectrometry (MS) analysis were as follows: the mobile phase was Methanol–Ammonium Acetate 10 mM aqueous solution (9:1, *v/v*); negative mode, electrospray ionization (ESI); probe temperature, 450°C; capillary voltage, 0.8 kV; cone voltage, 25 V.

Surface characterization of Ti implants

Scanning electron microscopy (SEM) was performed to highlight aspects related to the morphology of the samples, such as the size, particle shape, agglomeration tendency, and porous characteristics. Micrographs acquisitions were completed with the help of a high-resolution SEM (FEI Inspect F50) at 30 keV voltage and various magnifications. We used the same protocol for mesenchymal stem cells (MSCs) isolation described thoroughly in our previous work [10]. In order to analyze the cytotoxic and proliferation effect, the cultivation of both biomaterials with MSCs was performed, after prior ultraviolet (UV) sterilization of the implants. The biomaterials were seeded with MCSs for 48 hours, fixed in 2.5% Glutaraldehyde for one hour, washed with PBS, dehydrated through a graded series of ethanol, and vacuum dried. All samples were coated with gold using a sputter coater and the morphology of MSCs was observed by means of SEM (FEI Inspect F50).

Animals, anesthesia, and surgical technique

For our study, we used 10 male New Zealand White (NZW) rabbits aged six months, with an average weight of 3000–3500 g. All NZW rabbits were kept in animal facilities, at 25°C, having 12-hour of light:dark cycles. Throughout the entire experimental period, the rabbits were kept in individual plastic cages, and were provided a normal chow diet and water *ad libitum*.

The implantation and post-operative protocols followed by rabbit euthanasia for bone tissue harvesting has already been successfully used in other research projects and has been approved by the Ethics Committee of the University of Medicine and Pharmacy of Craiova (Approval No. 134/2019). During surgery, anesthesia was maintained by administration of Fentanyl diluted with saline (1 mL Fentanyl in 9 mL saline). General anesthesia was completed by administering 1% Lidocaine (5 mL) at the incision site. At the beginning of the surgical procedure, the incision site was depilated and washed well with water and soap as well as Betadine solution, after which the animal was covered with a sterile field. A 5 cm incision was performed at the anterior face of the proximal femoral region. This included the epidermis, dermis, and fascial layers and highlighted the femur covered by the periost. The periost

was incised and removed from the surface of the femur using a scraper. At the level of each femur, we made one excavation that completely removed the cortical bone near the medullary canal; for this, we used the Stryker Core Reamer orthopedic engine at low speed. In the femoral excavations, we inserted the implants (3 mm diameter, 5 mm long), as follows: in the left femur, we introduced HApTi (control implant); in the right femur, we introduced HApTiCaFb.

We chose the implantation of the two biocomposites in different femurs of the same animals to exclude variations owing to different animal healing responses. Subsequently, structure incisions were sutured with 4-0 Dexon thread. After the surgical procedure, we subcutaneously administered two doses of Buprenorphine diluted in saline at a dose of 0.05 mg/kg every four hours between doses. The operative wound was controlled and patched daily until healed. Prior to sacrifice, the rabbits were sedated by subcutaneous administration of Fentanyl (0.1 mL/kg) and Midazolam (2 mg/kg).

Histopathology and immunohistochemistry analysis

Histological tissue analysis was performed to observe the degree of composite osteointegration, osteoformation, and biocompatibility with bone tissue. Eight weeks after the implantation of the composites, the animals were sacrificed, and the femoral bones were removed and processed according to classical decalcification and paraffin embedding protocols.

Bone fragments were first decalcified for two months in 10% buffered ethylenediaminetetraacetic acid (EDTA; pH 7.4), with constant mechanical agitation on an orbital shaker. A fresh solution was prepared each week, and the decalcification endpoint was checked by testing the density of the bone fragment with a sharp metallic pointer, until the consistency was below that of cartilage. All tissue fragments had the same size (2×1×0.3 cm) and were decalcified for the same amounts of time.

After decalcification, tissue fragments were thoroughly washed in tap water, distilled water, dehydrated in increasing ethanol concentrations (75–100%), cleared in Xylene for three hours, and incubated in two paraffin baths, overnight, at 67°C. On the next day, the fragments were embedded in paraffin blocks that were sectioned at very low speed on a rotary microtome (Microm), producing 4 μm-thick sections that were collected on poly-L-Lysine coated slides.

For histological staining, the slides were deparaffinated, rehydrated and then stained sequentially in Hematoxylin and Eosin (HE) solutions. The sections were then dehydrated, cleared, and placed under coverslips utilizing a permanent Xylene-based mounting medium (Sigma-Aldrich).

For immunohistochemistry (IHC), the slides were deparaffinized, rehydrated, and processed for antigen retrieval by microwaving for 21 minutes, at 600 W. After cooling down to room temperature, endogenous peroxidase was inhibited with 1% hydrogen peroxide (H_2O_2) for 30 minutes, and unspecific antigenic binding sites were blocked with 3% skim milk. The samples were incubated with primary antibodies [1:50 dilution in 3% bovine serum albumin (BSA)–PBS], overnight, at 4°C. Primary antibodies were osteocalcin (OC; OCG3, #ab13420, Abcam, UK) and osteopontin (OPN; 1B20, #NB110-89062, Novus Biologicals, UK). On the next day, the sections were washed in 1× PBS, and a species-specific Horseradish Peroxidase (HRP)-labeled secondary antibody was added for one hour [ImmPRESS™ HRP Goat Anti-Mouse Immunoglobulin G (IgG) (Peroxidase) Polymer Detection Kit, Vector Lab]. After further washing in PBS, the signal was detected with 3,3'-Diaminobenzidine (DAB; Histofine® DAB-3S kit), and finally the slides were briefly counter-stained with Mayer's Hematoxylin, dehydrated, cleared, and placed under the coverslip with a Xylene-based mounting medium (Sigma-Aldrich) [15–17].

Results

CaFb coating analysis

To characterize the release of CaFb from the proposed biomaterial coatings, we immersed the biomaterials in a PBS physiological buffer, at 37°C. The sampled supernatants were quantified by HPTLC. The results showed that CaFb release occurred rapidly within the first 75 hours; then, it plateaued over a period of up to 14 days (Figure 1). Using MS analysis, the *m/z* values obtained for fructoborate anion and fructose were as follows: $[M\text{-}H]^-$ 367.12, fructoborate (main ion); $[M\text{-}H]^-$ 179.97, fructose (fragment) (Figure 2). The release time of CaFb is satisfactory, considering the simplicity and accessibility of the CD method.

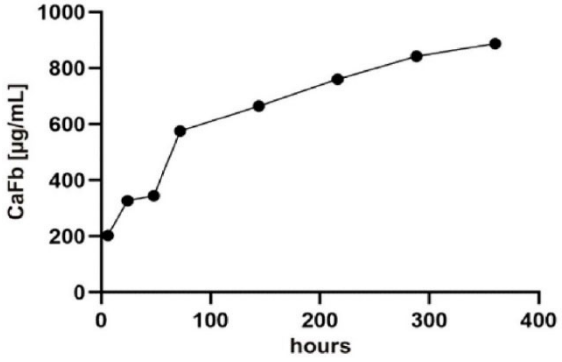

Figure 1 – ***CaFb release (in PBS, pH 7.4, at 37°C) from the biomaterials coating obtained by CD. The amount of released CaFb was quantified by HPTLC. CaFb: Calcium fructoborate; CD: Chemisorption deposition; HPTLC: High-performance thin-layer chromatography; PBS: Phosphate-buffered saline.***

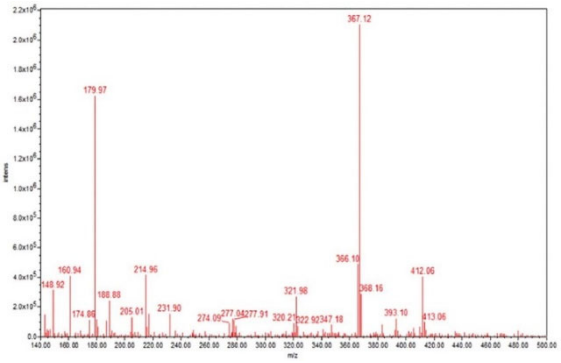

Figure 2 – ***MS profile of the released CaFb compound. CaFb: Calcium fructoborate; MS: Mass spectrometry.***

Analysis of coating surface morphology

Both implants showed a granular appearance on the ceramic surface, as determined by SEM analysis. In both cases, the presence of nanometric particles or agglomerates, most likely consisting of HAp, was uniformly dimensional. The morphology was predominantly spherical, but sometimes-smaller rods and polyhedral particles were present. Due to the method of obtaining implants using the TSS stage, the nanometric particles of HAp retain their size. Particle diameters ranged from 70 to 120 nm and were similar for both materials. Implants have low porosity, sometimes identifying triple junctions resulting from the bonding of several particles because of heat treatment applied (Figures 3 and 4).

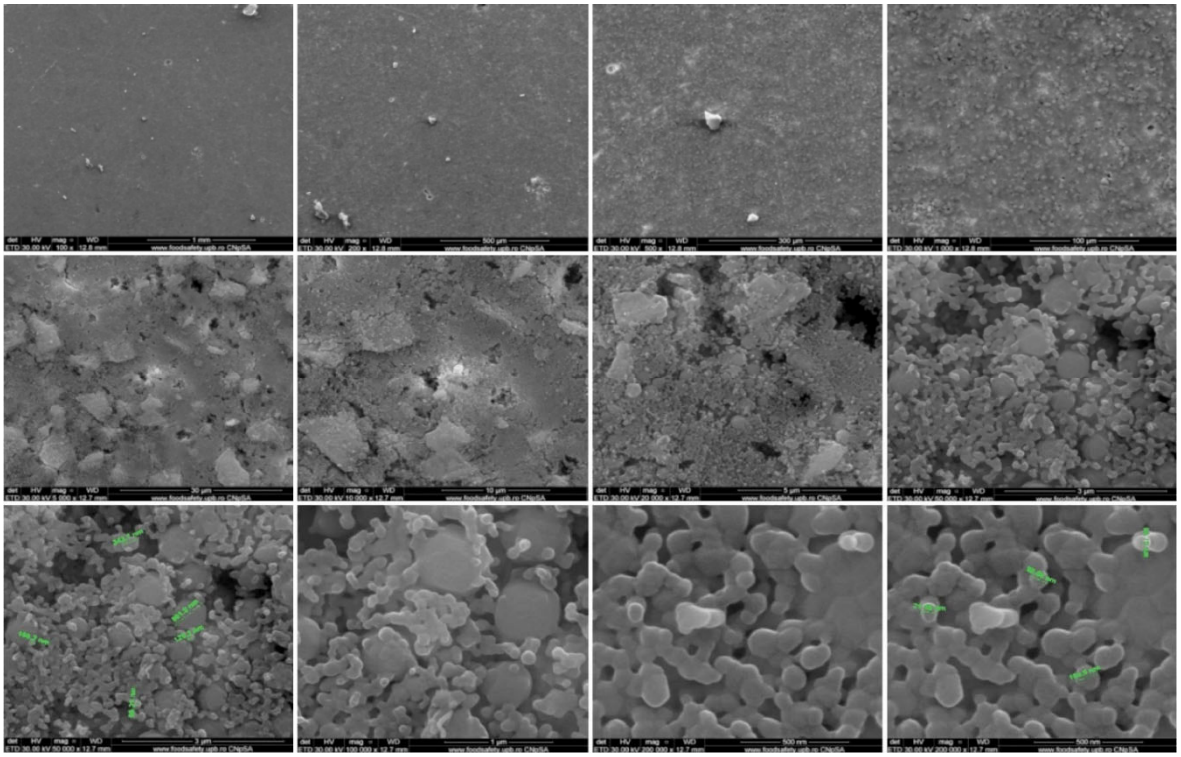

Figure 3 – ***SEM images of HApTi implants. HApTi: Hydroxyapatite-coated titanium; SEM: Scanning electron microscopy.***

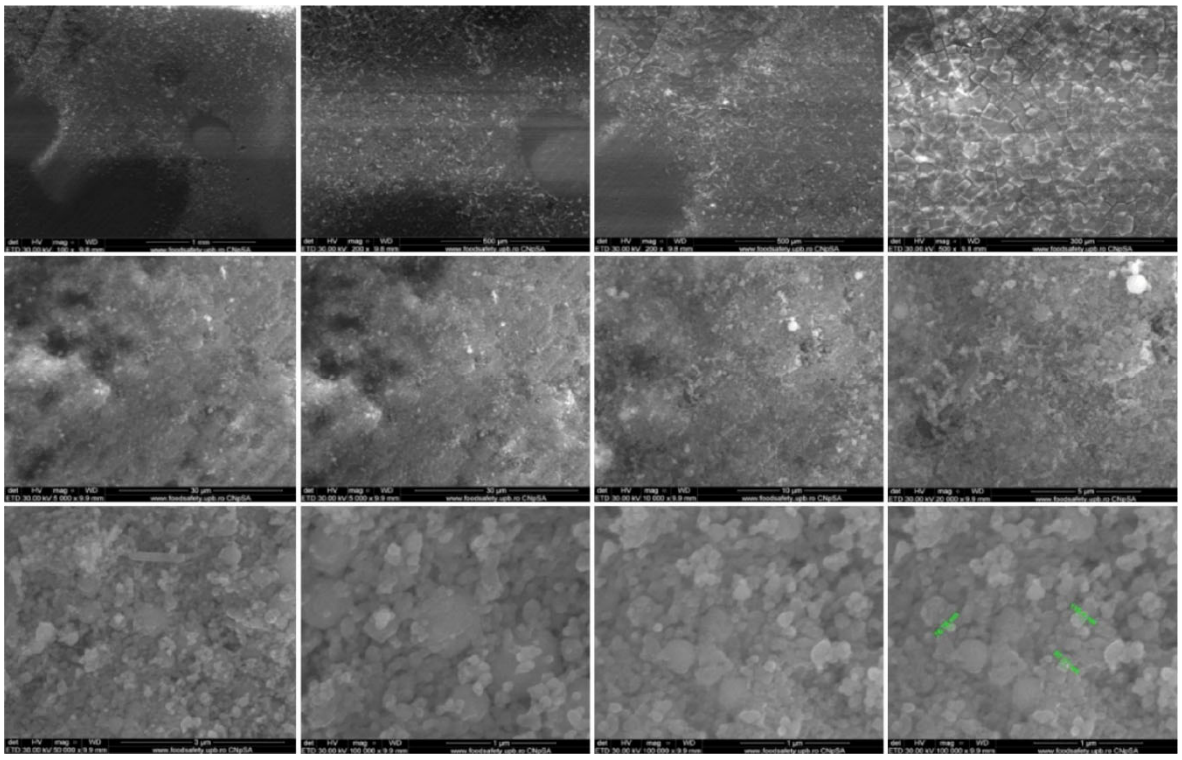

Figure 4 – ***SEM images of HApTiCaFb implants. HApTi: Hydroxyapatite-coated titanium; HApTiCaFb: Calcium fructoborate coating on a HApTi; SEM: Scanning electron microscopy.***

SEM analysis of Ti implants after *in vitro* study

Using the SEM technique, we tested the potential of composites to be substrates for the *in vitro* adhesion and growth of osteoblasts on their surface. It was observed that when using HApTi implants, the number of cells that adhered to the surface is small compared to HapTiCaFb (Figures 5 and 6). The addition of CaFb has a direct positive effect on the process of cell adhesion and growth. In the case of the HapTiCaFb sample, a high number of cells is found on the surface of the analyzed composite, of micron dimensions, with typical morphological appearance, which demonstrates a good adhesion to the substrate and a reduced cytotoxic effect of the material (Figure 6). Experimental data show that HApTiCaFb can promote cell proliferation and thus tissue and bone regeneration. Correlating the pharmacological effect of CaFb with SEM images, we can conclude that CaFb in the used concentration, stimulates cell adhesion and proliferation.

In vivo testing

Histopathology showed that the implants ended suddenly where the bone began, with no histological indication of newly formed bone tissue; neither fibrosis nor inflammation was observed. Characteristic elements of chronic inflammation (neutrophils, macrophages, foreign body giant cells) and necrosis were not detected up to eight weeks following initial implantation (Figure 7, a and b). Lack of osseointegration implant–bone elements visible with histology can be explained by lower maintenance period femur implant in animals studied.

IHC examination of the treated sections for OC and OPN immunoexpression was performed under both transmitted and polarized light to visualize osteoblasts and OC as non-collagenous protein (NCP) (Figures 8–11, a, c, e and g), as well as birefringent collagen fibers (Figures 8–11, b, d, f and h).

At the implant–bone interface of the left femur, we examined OC immunoexpression in osteoblasts, Havers channels, and bone lamellae. Following transmitted light microscopy analysis, we observed implant adhesion to the surface of the bone tissue, implant fragments embedded in bone mass, and the presence of newly formed collagen fibers. Polarized light images revealed the presence of birefringent collagen fibers that ensure the incorporation of implant fragments into the bone integration area (Figure 8, a–h).

The implant–bone interface of the right femur revealed the presence of OC in the extracellular bone matrix and Havers channels. Brightfield light examination showed the presence of implant fragments in the extracellular bone matrix and osteoblasts. When examined under polarized light, our analysis revealed the presence of birefringent collagen fibers (Figure 9, a–h).

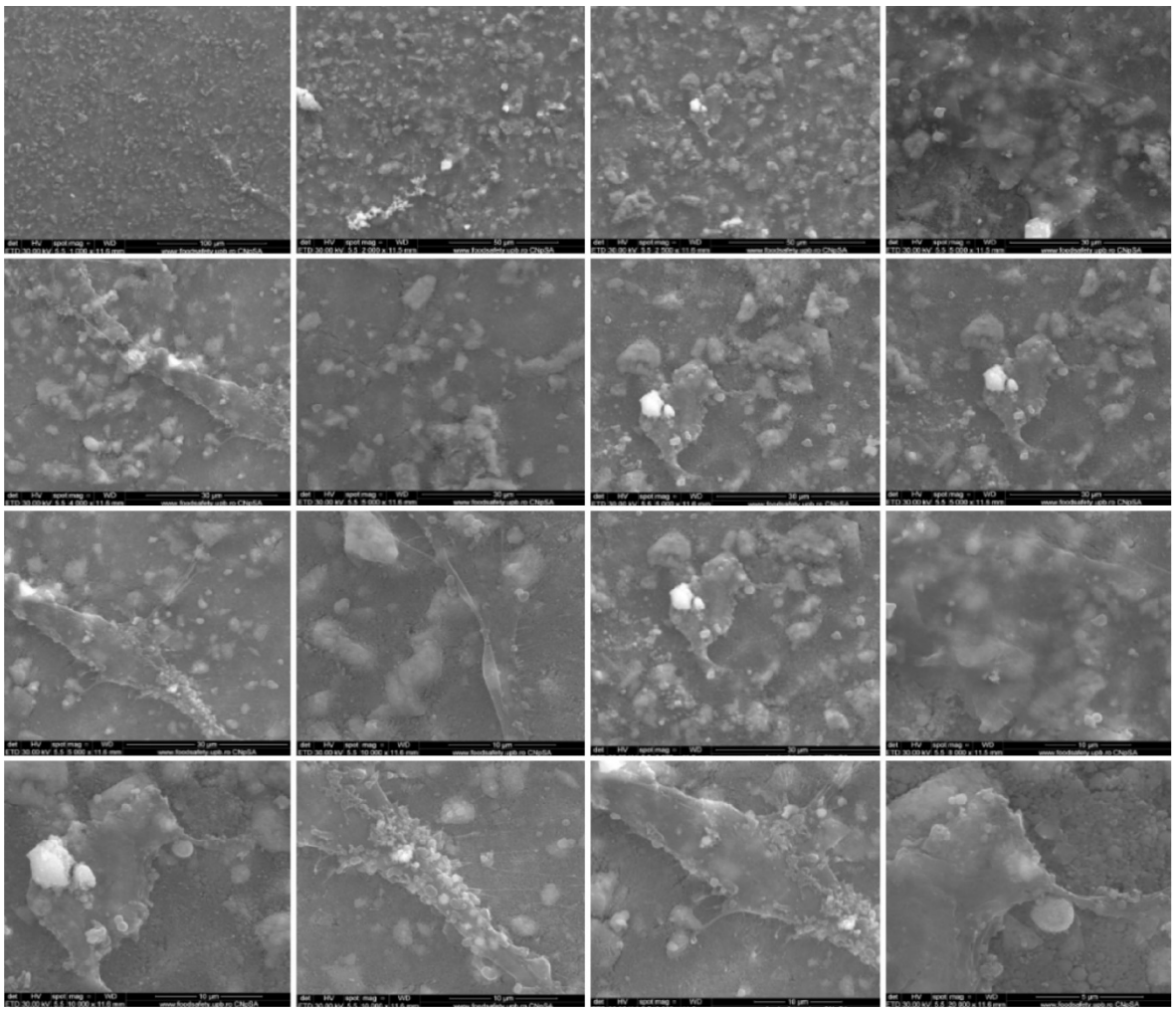

Figure 5 – ***SEM images of HApTi implants after in vitro study. HApTi: Hydroxyapatite-coated titanium; SEM: Scanning electron microscopy.***

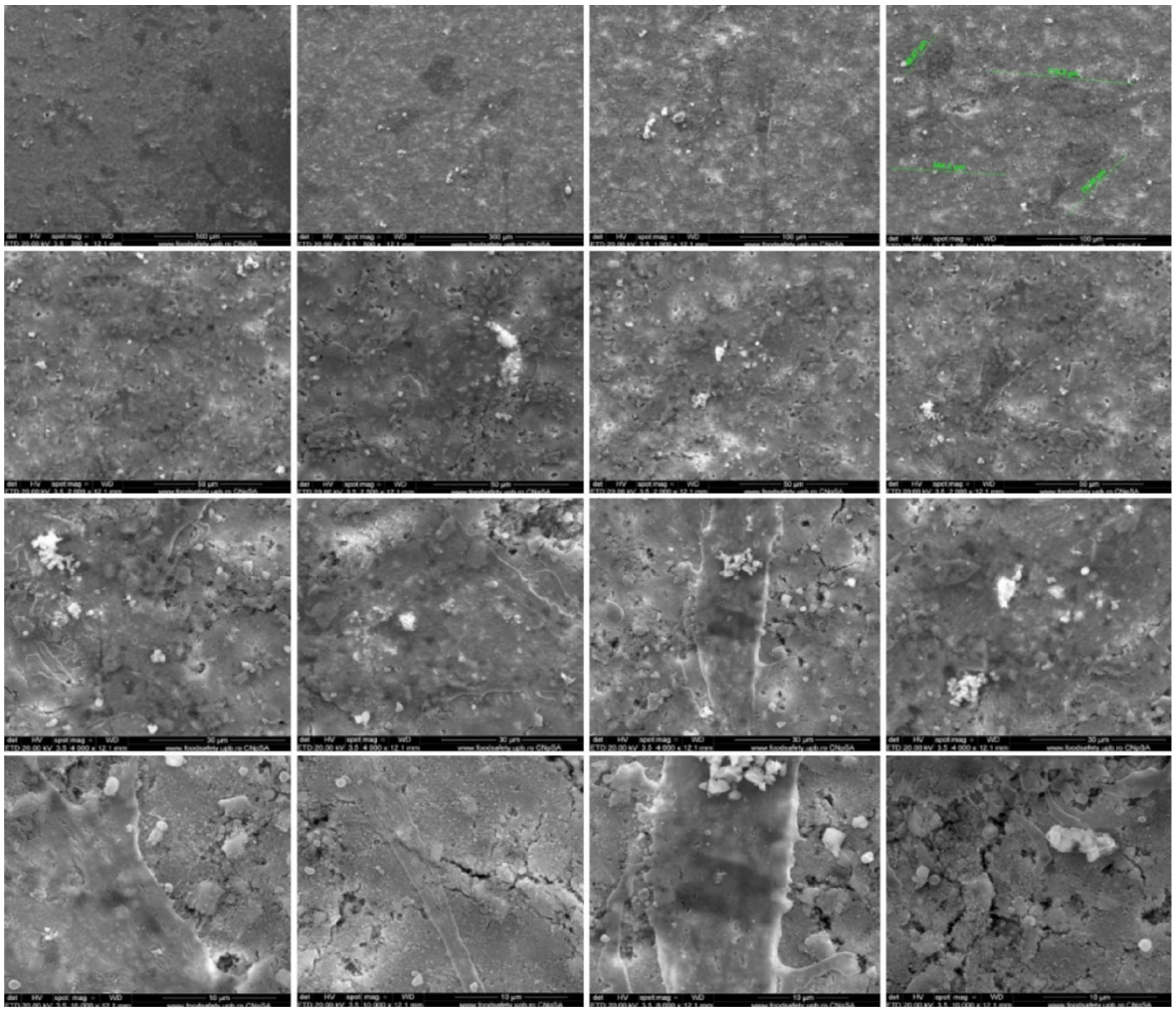

Figure 6 – ***SEM images of HApTiCaFb implants after in vitro study. HApTi: Hydroxyapatite-coated titanium; HApTiCaFb: Calcium fructoborate coating on a HApTi; SEM: Scanning electron microscopy.***

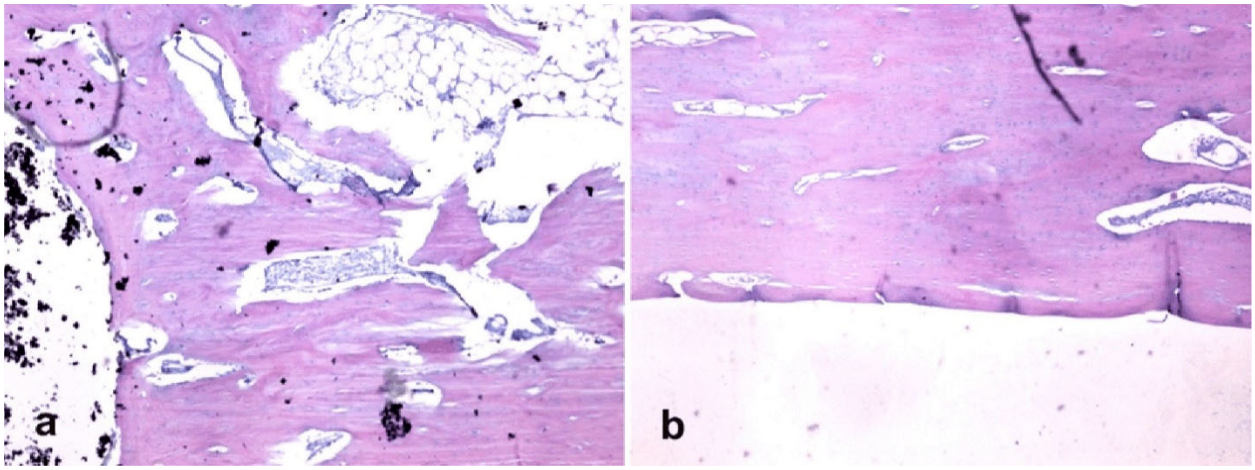

Figure 7 – ***Implant–bone interface histological analysis (HE staining, ×40): (a) HApTi (left femur); (b) HApTiCaFb (right femur). HApTi: Hydroxyapatite-coated titanium; HApTiCaFb: Calcium fructoborate coating on a HApTi; HE: Hematoxylin–Eosin.***

OPN appeared to be expressed in the left femur at the level of osteoblasts and the Havers canals. Brightfield light analysis of OPN indicated the presence of a partial adherence zone of the implant to the adjacent bone tissue and the presence of osteoblasts. Under polarized light, birefringent collagen fibers near the implant–bone interface were observed; however, birefringent collagen bundles were not detected in the implant incorporation area (Figure 10, a–h).

In the right femurs of the NZW rabbits, OPN was expressed in the extracellular bone matrix and Havers channels. In brightfield light analysis, we observed implant fragments adhering to the adjacent bone tissue and the presence of osteocytes. Under polarized light, collagen fibers and implant incorporation zones without the birefringence phenomenon were observed (Figure 11, a–h).

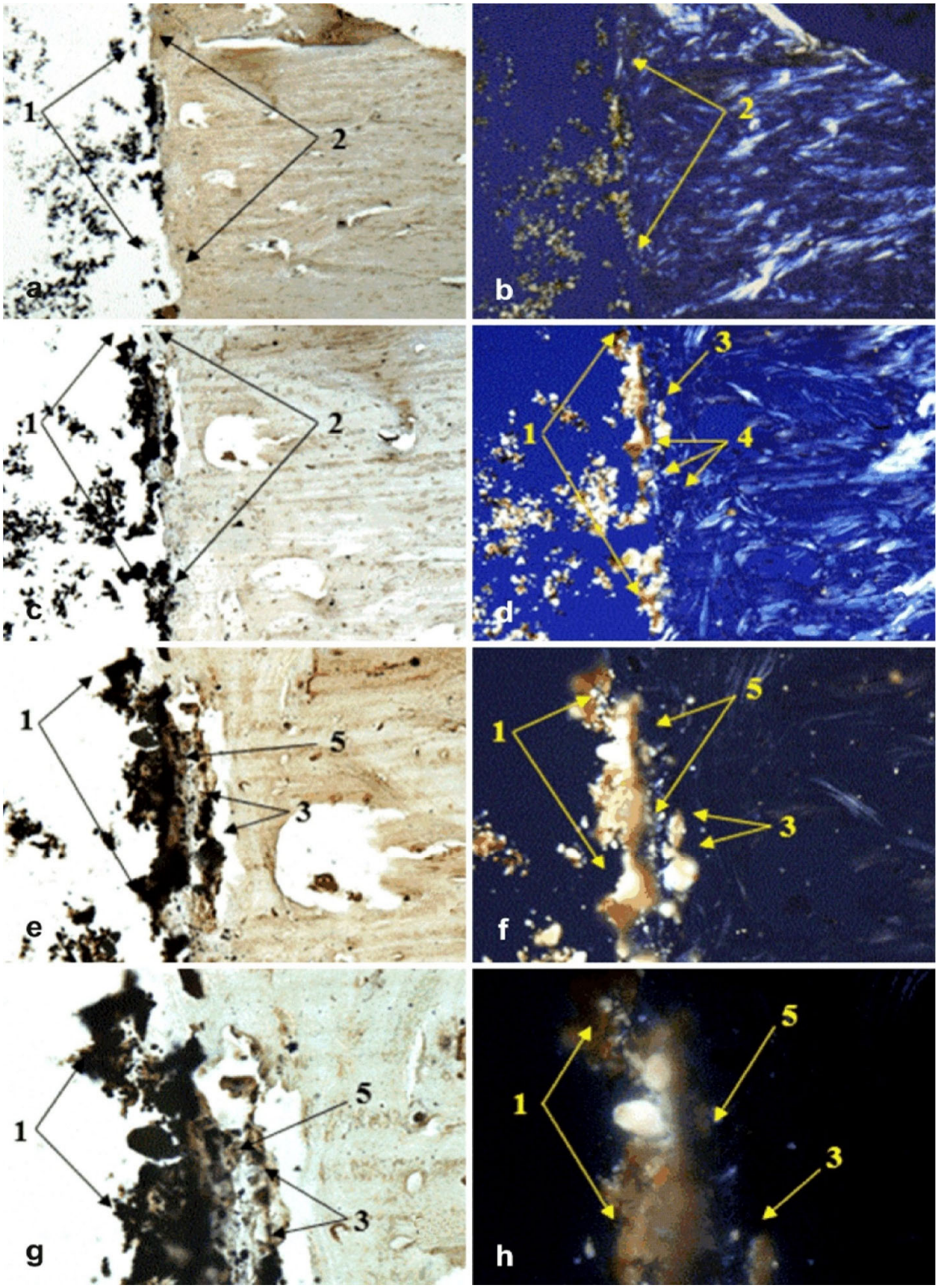

Figure 8 – ***Morphogenesis of implant integration into adjacent bone tissue: (a–h) Tissue surrounding the HApTi implant in the left femur was immunostained for OC. 1: Implant adhering to the bone surface; 2: Bone area of implant adhesion; 3: Implant fragment incorporated into the bone marrow; 4: Birefringent collagen fibers observed under polarized light ensure incorporation of implant fragments into the bone integration area; 5: Area occupied by neoformed collagen fibers. Anti-OC antibody immunostaining: (a and b) ×28; (c and d) ×140; (e and f) ×210; (g and h) ×280. HApTi: Hydroxyapatite-coated titanium; OC: Osteocalcin.***

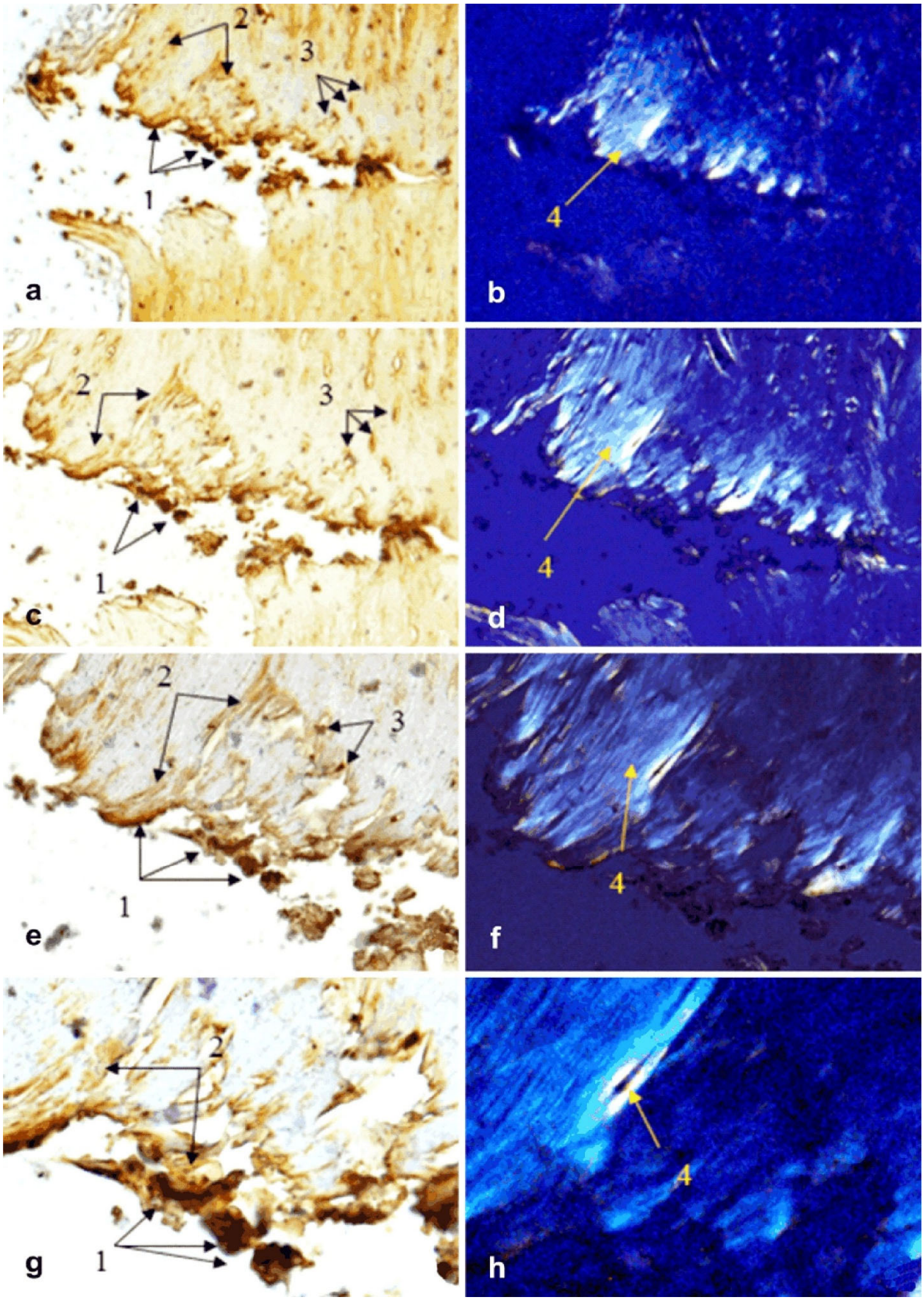

Figure 9 – ***Morphogenesis of implant integration into adjacent bone tissue: (a–h) Tissue surrounding the HApTiCaFb implant in the right femur was immunostained for OC. 1: Implant fragments incorporated into the extracellular matrix; 2: Extracellular matrix containing OC; 3: Osteoblasts; 4: Birefringent collagen fibers observed under polarized light examination. Anti-OC antibody immunostaining: (a and b) ×28; (c and d) ×140; (e and f) ×210; (g and h) ×280. HApTi: Hydroxyapatite-coated titanium; HApTiCaFb: Calcium fructoborate coating on a HApTi; OC: Osteocalcin.***

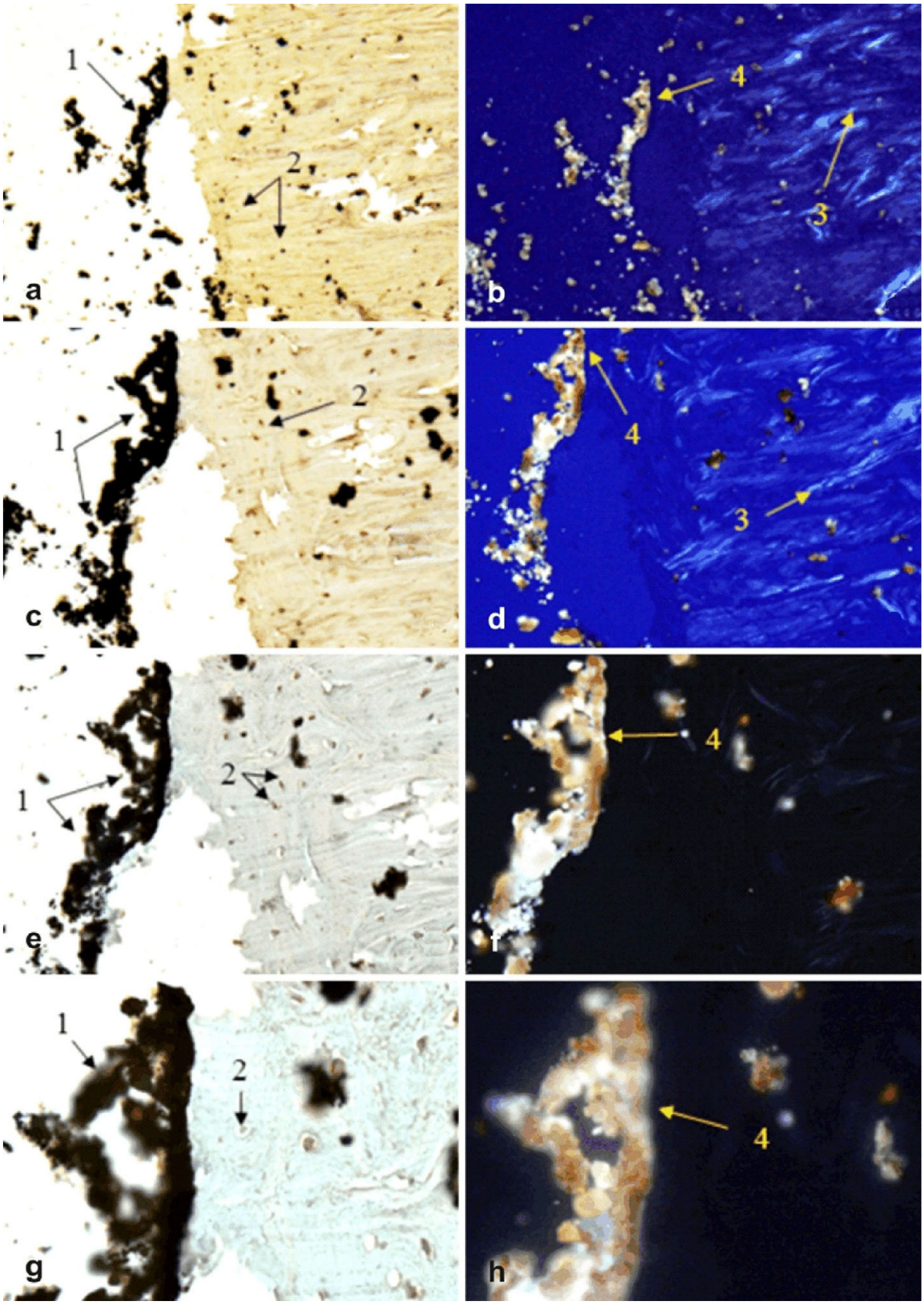

Figure 10 – ***Morphogenesis of implant integration into adjacent bone tissue: (a–h) Tissue surrounding the HApTi implant from the left femur was immunostained for OPN. 1: Partial adherent implant of adjacent bone tissue; 2: Osteoblasts; 3: Birefringent collagen fibers under polarized light examination; 4: Absence of birefringent collagen bundles in the implant incorporation area. Anti-OPN antibody immunostaining: (a and b) ×28; (c and d) ×140; (e and f) ×210; (g and h) ×280. HApTi: Hydroxyapatite-coated titanium; OPN: Osteopontin.***

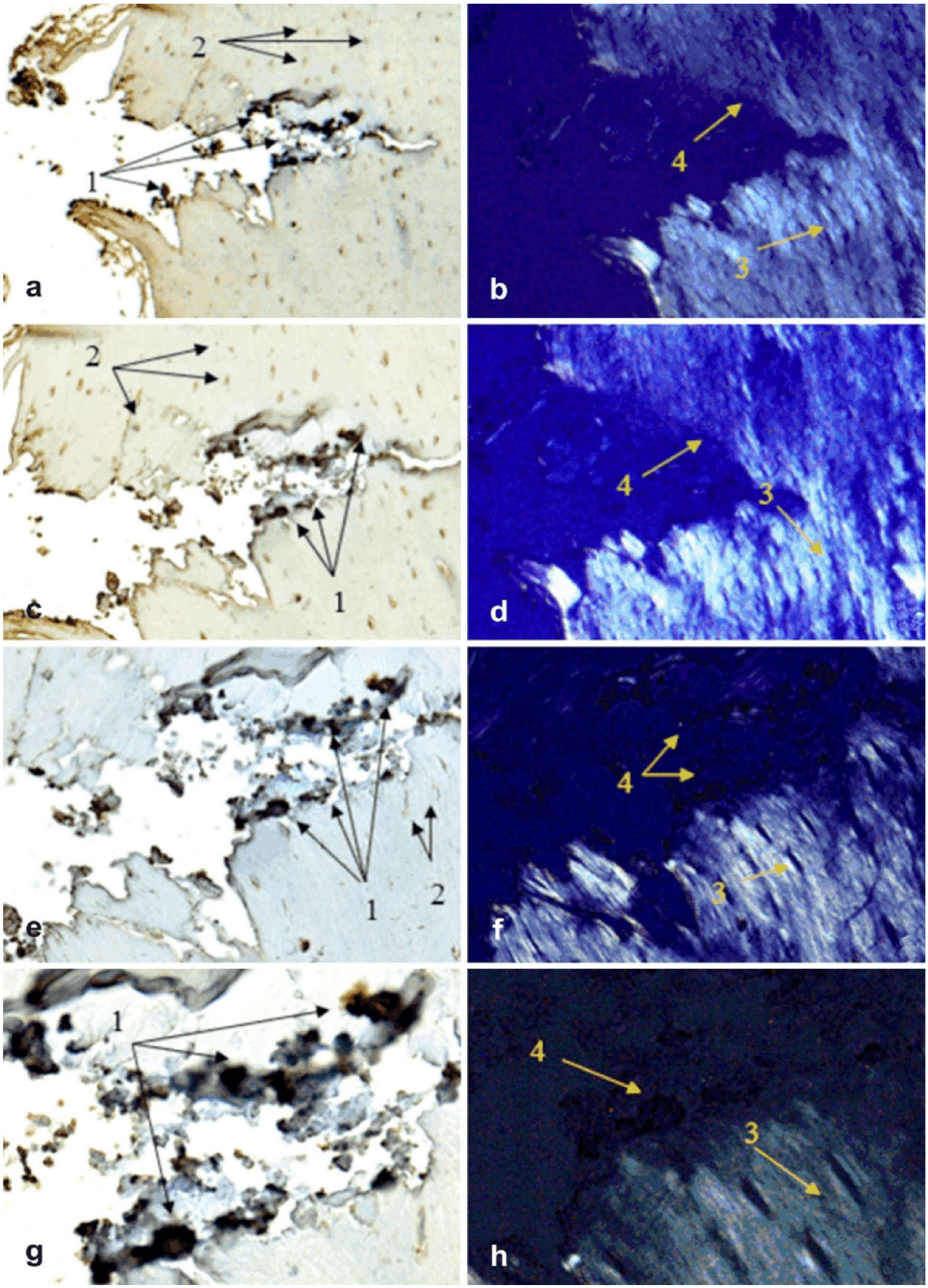

Figure 11 – ***Morphogenesis of implant integration into adjacent bone tissue: (a–h) Tissue surrounding the HApTiCaFb implant in the right femur was immunostained for OPN. 1: Adherent fragments of adjacent bone-bearing tissue; 2: Osteocytes; 3: Birefringent collagen fibers under polarized light examination; 4: Implant incorporation zone without the birefringence phenomenon. Anti-OPN antibody immunostaining: (a and b) ×28; (c and d) ×140; (e and f) ×210; (g and h) ×280. HApTi: Hydroxyapatite-coated titanium; HApTiCaFb: Calcium fructoborate coating on a HApTi; OPN: Osteopontin.***

For both types of implants tested, the analysis performed at the implant–bone interface reveals the adhesion areas of the implant, the implant fragments incorporated in the bone tissue mass, the birefringent collagen fibers, and the presence of osteoblasts. CaFb functionalization strategy significantly improves osseointegration, representing an interesting option for the treatment of osteoporotic fracture or other bone defects.

Discussions

The success of interventions involving the implantation of prostheses depends on the ability of the prosthesis components to rapidly fixate on the surface where the bone mass is located [18]. Because the opportunities for human studies are limited, a good alternative used by many researchers for the investigation of the implant–bone interface is represented by the using of the animal models [19]. This type of experiments comprises 35% of the rabbits used in medical research worldwide.

At the base of bone development stand three main mechanisms: modeling, remodeling, and longitudinal growth [20]. Adult bone remodeling is represented by a succession of events carried out by a group of cells that form bone multicellular units [21]. When osteoclasts are activated, they begin the bone resorption and erosion. When they have reached a certain depth of resorption, the osteoclasts will be replaced by mononuclear cells that will help complete the bone resorption [22]. After resorption, the area is invaded by preosteoblasts that differentiate into osteoblasts and begin the formation of the bone matrix. After a certain period (bone maturation time), the bone matrix will be mineralized into lamellar bone [23]. The osteoblasts will continue to form a bone matrix that will later mineralize, thus repairing the so-called resorption defect. During this process, some osteoblasts will be included into the matrix.

Resorption and formation are closely interconnected both temporally and spatially. In the normal remodeling phenomenon, the order of the processes is clearly determined, so the resorption will always be followed by formation, and formation will always be preceded by resorption [24]. An important parameter is represented by the bone balance, which stands for the difference between the amount of resorbed and reformed bone during the remodeling cycle. This parameter may vary on different surfaces of the bone and is influenced by a range of factors, both local and systemic [25].

The superior osseointegration of the HApTiCaFb implant in the rabbit femur can be explained by the release of CaFb over a period of two weeks. Barna *et al.* (2015), in other biological assays, suggest that HApCaFb biocomposites are potential materials that can prevent further bone loss and could increase or restore bone mass [8]. The release time of CaFb is satisfactory, considering the simplicity and accessibility of the CD method. Moreover, our recent research indicates that HApTi and HApTiCaFb exhibit a good *in vitro* biocompatibility on osteoprogenitor cell culture [10].

Woven bone is found in different processes, such as the process of rapid ossification, during fracture development and healing, or in different tumors and some bone metabolic disorders. The isotropic mechanical characteristics of the woven bone are given by the disorientation of collagen fibers [26]. Osteocyte is considered to be the most mature or most differentiated cell of the osteoblastic line, located in lacunae and interconnected by canals. Through cytoplasmic extensions inside canal cells, cells feed and maintain contact with other osteocytes or with cells from the bone surface [27]. On woven or immature bone, collagen fibers are randomly arranged. The structure of lamellar bone is characterized by the placement of the collagen fibers in parallel sheets and spindles, and the alternating orientation between the successive blades. This structure explains the variation of bright and dark bands seen under polarized light [28]. Histological analysis of the implant–bone interface revealed lack of inflammation and good biocompatibility for both implants.

OC and OPN are two major NCPs that are involved in the organization and deposition of the bone matrix, having important roles in both the mechanical and biological functions of bone. Both are expressed in the bone formation process and control bone mass, mineral size, and orientation [29]. To emphasize osteointegration and osteoformation, we performed IHC analysis. In left femurs, OC was expressed in osteoblasts, Havers channels, and bone lashes; OPN was expressed in osteoblasts and Havers channels. For the right femurs, OC and OPN were expressed in the extracellular bone matrix and Havers channels.

Analysis at the implant–bone interface for both types of implants reveals adhesion areas of the implant, implant fragments embedded in the mass of bone tissue, birefringent collagen fibers, and the presence of osteoblasts. Functionalization strategies significantly improve osseointegration, representing an interesting option for the treatment of osteoporotic fracture or other bone defects. Although these advances are yet to be fully applied clinically, functionalization represents a promising strategy to help improve the implant stability and to ensure fast, functional improvement in patient quality of life [30].

Recently, Tao *et al.* (2020) suggested that local incorporation of Acetylsalicylic Acid into HAp-coated Ti implants is useful to improve osseointegration by increasing bone formation around the implant through the activation of Notch signaling pathways, both in the osteoporotic and normal condition [31]. In addition, current animal studies demonstrate a possible improvement of osseointegration of the orthopedic implant in animal models from both systemic and local administration of Zoledronate [32].

In other experimental tests using ovariectomized rat animal model, there was evidence that bisphosphonates induced extracortical subperiosteal femur bone neoformation [33]. Another study indicates that the fixation of porous coated implants that have also been subject to HAp-surface coating and peri-implant bone compaction can be improved from local Alendronate treatment. Also, a beneficial role for HAp-coated joint replacements can be taken from the combined effect of local bisphosphonate treatment and bone compaction [34].

Another study found that local administration of Silymarin managed to stimulate bone formation around the implant in osteoporotic rats. The helpful effects of

Silymarin were proved through different parameters like increased implant osseointegration, binding strength, osteogenic activity, and improved trabecular microarchitecture. Thus, the fixation of HAp-coated implants in ovariectomized rats is improved by the local incorporation of Silymarin [35].

Conclusions

Our study showed that CaFb coatings can easily be applied by the CD method and that CaFb coatings have a promoting effect on implant osseointegration in the femurs of NZW rabbit experimental model. Both types of implants showed a good degree of osseointegration; however, several improvements support the superior osseointegration of HApTiCaFb implants and the possibility of using them in orthopedic surgery for bone reconstruction.

Conflict of interests

The authors declare that they have no conflict of interests.

Research involving human biological material

The study was performed in accordance with the ethical standards as laid down in the 1964 Declaration of Helsinki and its later amendments or comparable ethical standards. The written informed consent was obtained from all subjects included in the study. All the experimental procedures were approved by the Hospital's Ethics Committee (Approval No. 68/2016).

Research involving animals

All applicable international, national, and institutional guidelines for the care and use of animals were followed. All procedures performed in studies involving animals were in accordance with the ethical standards of the institution or practice at which the studies were conducted. All the experimental procedures were approved by the local Bioethics Committee for Animal Studies (Approval No. 134/2019).

Acknowledgments

This work was supported by a grant of the Romanian Ministry of Education and Research, CNCS–UEFISCDI, project number PN-III-P1-1.1-PD-2019-0214, within PNCDI III.

References

[1] Saleh KJ, Mulhall KJ, Hofmann AA, Bolognesi MP, Laskin RS. Primary total knee arthroplasty outcomes. In: Barrack RL, Booth RE Jr, Lonner JH, McCarthy JC, Mont MA, Rubash HE (eds). Orthopaedic knowledge update 3 – hip and knee reconstruction. 3rd edition, American Academy of Orthopaedic Surgeons, Rosemont, IL, USA, 2006, 93–110.

[2] Sporer S, Paprosky WG, Berry DJ. Hip revision. In: Barrack RL, Booth RE Jr, Lonner JH, McCarthy JC, Mont MA, Rubash HE (eds). Orthopaedic knowledge update 3 – hip and knee reconstruction. 3rd edition, American Academy of Orthopaedic Surgeons, Rosemont, IL, USA, 2006, 457–474.

[3] Kattimani VS, Kondaka S, Lingamaneni KP. Hydroxyapatite – past, present, and future in bone regeneration. Bone Tissue Regen Insights, 2016, 7:9–19. https://doi.org/10.4137/BTRI.S36138

[4] Rotaru LT, Varut RM, Nicolaescu O, Bubulica M, Belu I. *In vitro* release studies of alendronate from HA-AL composite deposited on titanium metal substrate. J Sci Arts, 2019, 19(2):443–448. http://www.josa.ro/docs/josa_2019_2/b_02_Varut_443-448_6p.pdf

[5] Chu C, Xue X, Zhu J, Yin Z. Mechanical and biological properties of hydroxyapatite reinforced with 40 vol. % titanium particles for use as hard tissue replacement. J Mater Sci Mater Med, 2004, 15(6):665–670. https://doi.org/10.1023/b:jmsm.0000030207.16887.f2 PMID: 15346733

[6] Hunter JM, Nemzer BV, Rangavajla N, Biţă A, Rogoveanu OC, Neamţu J, Scorei IR, Bejenaru LE, Rău G, Bejenaru C, Mogoşanu GD. The fructoborates: part of a family of naturally occurring sugar–borate complexes – biochemistry, physiology, and impact on human health: a review. Biol Trace Elem Res, 2019, 188(1):11–25. https://doi.org/10.1007/s12011-018-1550-4 PMID: 30343480 PMCID: PMC6373344

[7] Donoiu I, Militaru C, Obleagă O, Hunter JM, Neamţu J, Biţă A, Scorei IR, Rogoveanu OC. Effects of boron-containing compounds on cardiovascular disease risk factors – a review. J Trace Elem Med Biol, 2018, 50:47–56. https://doi.org/10.1016/j.jtemb.2018.06.003 PMID: 30262316

[8] Barna AS, Ciobanu G, Luca C, Luca AC. Nanohydroxyapatite–calcium fructoborate composites: synthesis and characterization. Rev Chim (Bucharest), 2015, 66(10):1618–1621. https://revistadechimie.ro/pdf/BARNA%20A.pdf%2010%2015.pdf

[9] Ciocilteu MV, Mocanu AG, Mocanu A, Ducu C, Nicolaescu OE, Manda VC, Turcu-Stiolica A, Nicolicescu C, Melinte R, Balasoiu M, Croitoru O, Neamtu J. Hydroxyapatite–ciprofloxacin delivery system: synthesis, characterisation and antibacterial activity. Acta Pharm, 2018, 68(2):129–144. https://doi.org/10.2478/acph-2018-0011 PMID: 29702474

[10] Sima LE, Varut RM, Gingu O, Sima G, Teisanu C, Neamtu J. *In vitro* characterization of hydroxyapatite-based biomaterials, using mesenchymal stem cell cultures from human bone marrow. J Sci Arts, 2020, 53(4):969–976. https://doi.org/10.46939/J.Sci.Arts-20.4-b02

[11] Gingu O, Benga G, Olei A, Lupu N, Rotaru P, Tanasescu S, Mangra M, Ciupitu I, Pascu I, Sima G. Wear behaviour of ceramic biocomposites based on hydroxiapatite nanopowders. Proc Inst Mech Eng E J Process Mech Eng, 2011, 225(1):62–71. https://doi.org/10.1243/09544089JPME307

[12] Gingu O, Cojocaru D, Ristoscu C, Sima G, Teisanu C, Mangra M. The influence of the foaming agent on the mechanical properties of the PM hydroxyapatite-based biocomposites processed by two-step sintering route. J Optoelectron Adv Mater, 2015, 17(7–8):1044–1049. https://joam.inoe.ro/articles/the-influence-of-the-foaming-agent-on-the-mechanical-properties-of-the-pm-hydroxyapatite-based-biocomposites-processed-by-two-step-sintering-route/fulltext

[13] Rotaru P, Scorei R, Hărăbor A, Dumitru MD. Thermal analysis of a calcium fructoborate sample. Thermochim Acta, 2010, 506(1–2):8–13. https://doi.org/10.1016/j.tca.2010.04.006

[14] Bita A, Mogosanu GD, Bejenaru LE, Oancea CN, Bejenaru C, Croitoru O, Rau G, Neamtu J, Scorei ID, Scorei IR, Hunter J, Evers B, Nemzer B, Anghelina F, Rogoveanu OC. Simultaneous quantitation of boric acid and calcium fructoborate in dietary supplements by HPTLC–densitometry. Anal Sci, 2017, 33(6):743–746. https://doi.org/10.2116/analsci.33.743 PMID: 28603198

[15] Zimta D, Melinte PR, Dinca I, Dragoi GS. Anatomic markers for the retrospective and prospective evaluation of pathology involving the feto-placental and utero-placental circulatory systems inside human placenta. Forensic implications. Rom J Leg Med, 2012, 20(1):19–32. https://doi.org/10.4323/rjlm.2012.19

[16] Varut RM, Gîrd CE, Rotaru LT, Varut MC, Pisoschi CG. Evaluation of polyphenol and flavonoid profiles and the antioxidant effect of *Carduus acanthoides* hydroalcoholic extract compared with *Vaccinium myrtillus* in an animal model of diabetes mellitus. Pharm Chem J, 2018, 51(12):1088–1095. https://doi.org/10.1007/s11094-018-1746-0

[17] Haragus H, Prejbeanu R, Patrascu J, Faur C, Roman M, Melinte R, Timar B, Codorean I, Stetson W, Marra G. Cross-cultural adaptation and validation of the Romanian Oxford Shoulder Score. Medicine (Baltimore), 2018, 97(23):e10926. https://doi.org/10.1097/MD.0000000000010926 PMID: 29879033 PMCID: PMC5999452

[18] Isaacson BM, Jeyapalina S. Osseointegration: a review of the fundamentals for assuring cementless skeletal fixation. Orthop Res Rev, 2014, 6:55–65. https://doi.org/10.2147/ORR.S59274

[19] Pearce AI, Richards RG, Milz S, Schneider E, Pearce SG. Animal models for implant biomaterial research in bone: a review. Eur Cell Mater, 2007, 13:1–10. https://doi.org/10.22203/ecm.v013a01 PMID: 17334975
[20] Setiawati R, Rahardjo P. Bone development and growth. In: Yang H (ed). Osteogenesis and bone regeneration. IntechOpen Ltd., London, 2018, 1–15. https://doi.org/10.5772/intechopen.82452
[21] Rucci N. Molecular biology of bone remodelling. Clin Cases Miner Bone Metab, 2008, 5(1):49–56. PMID: 22460846 PMCID: PMC2781193
[22] Teitelbaum SL. Bone resorption by osteoclasts. Science, 2000, 289(5484):1504–1508. https://doi.org/10.1126/science.289.5484.1504 PMID: 10968780
[23] Shapiro F. Bone development and its relation to fracture repair. The role of mesenchymal osteoblasts and surface osteoblasts. Eur Cell Mater, 2008, 15:53–76. https://doi.org/10.22203/ecm.v015a05 PMID: 18382990
[24] Jarcho M, Kay JF, Gumaer KI, Doremus RH, Drobeck HP. Tissue, cellular and subcellular events at a bone–ceramic hydroxylapatite interface. J Bioeng, 1977, 1(2):79–92. PMID: 355244
[25] Florencio-Silva R, da Silva Sasso GR, Sasso-Cerri E, Simões MJ, Cerri PS. Biology of bone tissue: structure, function, and factors that influence bone cells. Biomed Res Int, 2015, 2015:421746. https://doi.org/10.1155/2015/421746 PMID: 26247020 PMCID: PMC4515490
[26] Serra-Vinardell J, Roca-Ayats N, De-Ugarte L, Vilageliu L, Balcells S, Grinberg D. Bone development and remodeling in metabolic disorders. J Inherit Metab Dis, 2020, 43(1):133–144. https://doi.org/10.1002/jimd.12097 PMID: 30942483
[27] Dallas SL, Prideaux M, Bonewald LF. The osteocyte: an endocrine cell … and more. Endocr Rev, 2013, 34(5):658–690. https://doi.org/10.1210/er.2012-1026 PMID: 23612223 PMCID: PMC3785641
[28] Martin RB, Lau ST, Mathews PV, Gibson VA, Stover SM. Collagen fiber organization is related to mechanical properties and remodeling in equine bone. A comparison of two methods. J Biomech, 1996, 29(12):1515–1521. https://doi.org/10.1016/S0021-9290(96)80002-9 PMID: 8945649
[29] Bailey S, Karsenty G, Gundberg C, Vashishth D. Osteocalcin and osteopontin influence bone morphology and mechanical properties. Ann N Y Acad Sci, 2017, 1409(1):79–84. https://doi.org/10.1111/nyas.13470 PMID: 29044594 PMCID: PMC5730490
[30] Sartori M, Maglio M, Tschon M, Aldini NN, Visani A, Fini M. Functionalization of ceramic coatings for enhancing integration in osteoporotic bone: a systematic review. Coatings, 2019, 9(5):312. https://doi.org/10.3390/coatings9050312
[31] Tao Z, Zhou W, Wu X, Lu H, Ma N, Li Y, Zhang R, Yang M, Xu HG. Local administration of aspirin improves osseointegration of hydroxyapatite-coated titanium implants in ovariectomized rats through activation of the Notch signaling pathway. J Biomater Appl, 2020, 34(7):1009–1018. https://doi.org/10.1177/0885328219889630 PMID: 31757183
[32] He Y, Bao W, Wu XD, Huang W, Chen H, Li Z. Effects of systemic or local administration of zoledronate on implant osseointegration: a preclinical meta-analysis. Biomed Res Int, 2019, 2019:9541485. https://doi.org/10.1155/2019/9541485 PMID: 31663000 PMCID: PMC6778941
[33] Canettieri ACV, Colombo CED, Chin CM, Faig-Leite H. Femur bone repair in ovariectomized rats under the local action of alendronate, hydroxyapatite and the association of alendronate and hydroxyapatite. Int J Exp Pathol, 2009, 90(5):520–526. https://doi.org/10.1111/j.1365-2613.2009.00674.x PMID: 19765106 PMCID: PMC2768150
[34] Jakobsen T, Baas J, Kold S, Bechtold JE, Elmengaard B, Søballe K. Local bisphosphonate treatment increases fixation of hydroxyapatite-coated implants inserted with bone compaction. J Orthop Res, 2009, 27(2):189–194. https://doi.org/10.1002/jor.20745 PMID: 18752278 PMCID: PMC3707404
[35] Tao ZS, Wu XJ, Yang M, Xu HG. Local administration with silymarin could increase osseointegration of hydroxyapatite-coated titanium implants in ovariectomized rats. J Biomater Appl, 2019, 34(5):664–672. https://doi.org/10.1177/0885328219863290 PMID: 31342833

Corresponding author
Ion Romulus Scorei, Professor, Biochem, PhD, Department of Biochemistry, BioBoron Research Institute, S.C. Natural Research S.R.L., 31B Dunării Street, 207465 Podari, Dolj County, Romania; Phone +40351–407 543, e-mail: romulus_ion@yahoo.com

Received: June 30, 2020

Accepted: June 23, 2021